Effects of current on nanoscale ring-shaped magnetic tunnel junctions

Hong-Xiang Wei,[1] Jiexuan He,[2] Zhen-Chao Wen,[1] Xiu-Feng Han,[1,†] Wen-Shan Zhan,[1] and Shufeng Zhang[2,*,‡]
[1]*State Key Laboratory of Magnetism, Beijing National Laboratory for Condensed Matter Physics, Institute of Physics, Chinese Academy of Science, Beijing 100080, China*
[2]*Department of Physics and Astronomy, University of Missouri, Columbia, Missouri 65211, USA*
(Received 6 March 2008; published 17 April 2008)

We report the observation and micromagnetic analysis of current-driven magnetization switching in nanoscale ring-shaped magnetic tunnel junctions. When the electric current density exceeds a critical value of the order of 6×10^6 A/cm^2, the magnetization of the two magnetic rings can be switched back and forth between parallel and antiparallel onion states. Theoretical analysis and micromagnetic simulation show that the dominant mechanism for the observed current-driven switching is the spin torque rather than the current-induced circular Oersted field.

DOI: 10.1103/PhysRevB.77.134432 PACS number(s): 75.47.De, 73.50.Jt, 75.75.+a

I. INTRODUCTION

In the experiments that demonstrated current-driven magnetization switching for spin valve pillars[1] or magnetic tunnel junctions (MTJs),[2] magnetic elements have been patterned into elliptic or rectangular shapes. Undesired properties such as a large shape anisotropy and a strong stray field would place a severe limitation on these magnetic elements for ultrahigh density memory devices. The ring-shaped spin valve or MTJ eliminates the stray field and enhances the thermal stability since the magnetization may ideally form a vortex structure free of magnetic poles.[3–5] Recently, the magnetic rings made of a single magnetic layer[6–8] and of spin valves[9–13] have been achieved. For the current in the plane (CIP) of the layers, the measurement of the CIP resistance of the spin valve probes the domain structure of the free layer.[9] For the current perpendicular to the plane of the layers, the magnetization can be switched by the current.[11–13] In these studies, the size of the rings ranged from submicrometers to micrometers and the current-induced Oersted field is the dominant mechanism in switching. To achieve the switching by the spin transfer torque,[14] it is necessary to make the ring size of the order of 100 nm or less. We had previously reported the fabrication and measurement of ring-shaped magnetic tunnel junctions,[15] where the fixed layer is pinned by an antiferromagnetic layer.

In the present work, we have successfully made a series of the ring-shaped MTJ structures with various ring diameters and without an antiferromagnetic layer; this simpler layer structure makes the analysis more straightforward. Our micromagnetic simulation shows that the observed magnetization switching is originated from spin transfer torques and the current-induced circular Oersted field plays very minor roles in switching. Although the desired vortex states have not been identified in our experiments and simulation, the definitive verification of the switching between onion states (described in detail later) by the spin torque is encouraging for a further exploration of the geometrically controlled magnetic states.

II. EXPERIMENTAL PROCEDURES

Multilayered MTJ films with the hard-ferromagnetic/insulator/soft-ferromagnetic layer structure of Ta(5 nm)/Cu(20 nm)/Ta(5 nm)/$Co_{50}Fe_{50}$(2.5 nm)/Al(0.6 nm)oxide/$Co_{60}Fe_{20}B_{20}$(2.5 nm)/Ta(3 nm)/Ru(5 nm) were deposited on the Si(100)/SiO_2 substrate by using an ULVAC TMR R & D Magnetron Sputtering System (MPS-4000-HC7) with a base pressure of 1×10^{-6} Pa. The Al-oxide barrier was fabricated by inductively coupled plasma oxidizing a 0.6 nm Al layer with an oxidation time of 10 s in a mixture of oxygen and argon at a pressure of 1.0 Pa in a separate chamber. Two electrodes situated above and below the nanoring MTJ were patterned by ultraviolet optical lithography combined with Ar-ion beam milling.[16,17] The active ring-shaped junction area was patterned by electron beam lithography using a Raith 150 scanning electron microscope (SEM) and reactive ion etching. The nanoring MTJ pillar including the top resist was then buried by SiO_2 deposition. Finally, the resist and SiO_2 on the top of a nanoring were removed by using a lift-off process before the top electrode was patterned in the perpendicular direction.

The transport measurement was conducted via a standard four-probe method. The tunnel resistance was measured by applying a small current (10 μA) so that the magnetic state of the ring is not disturbed.

III. EXPERIMENTAL RESULTS AND MICROMAGNETIC ANALYSIS

Figures 1(a) and 1(b) show the SEM images of an array of ring-shaped MTJs and of a single MTJ whose inner and outer diameters are about 50 and 100 nm, respectively. The magnetization state of a deep submicron-sized single ring has two possible stable configurations at zero external magnetic field (remanent state): onion (O) and vortex (V), as shown in Fig. 1(d). The onion states are metastable states; they can easily be formed via the application of an in-plane magnetic field. Each onion state has a pair of domain walls; in the presence of a large uniaxial anisotropy, two domain walls are pinned around the easy axis. If the anisotropy is small, the magnetostatic interaction between two domain walls tends to attract each other, forming a slightly asymmetric onion state (not shown). The vortex state is the lowest energy state and is more stable than the O state. However, there is no simple experimental method available to produce

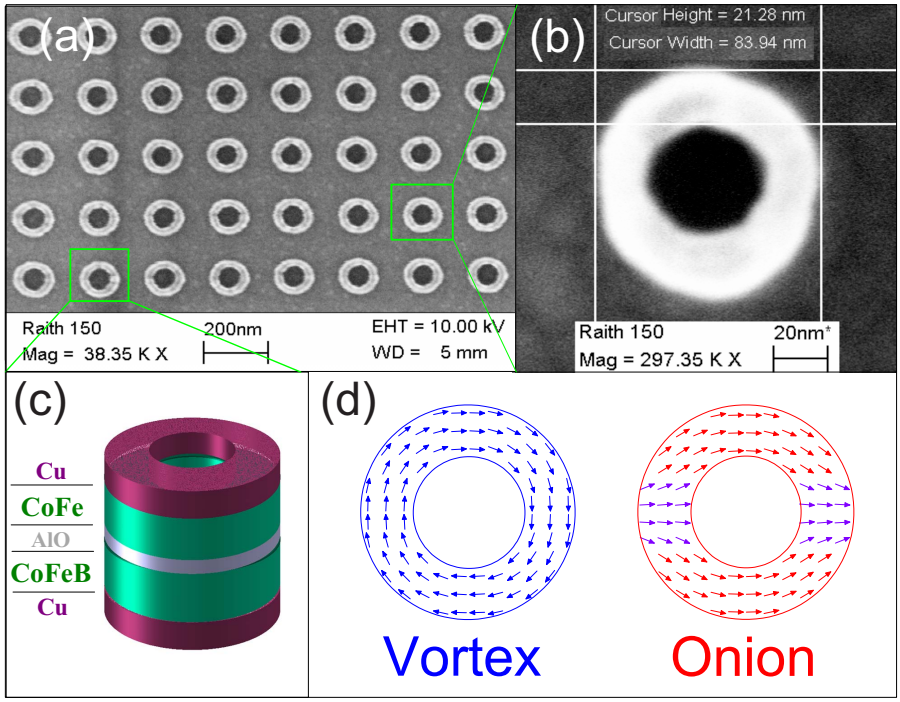

FIG. 1. (Color online) The SEM images of the (a) array and (b) single magnetic tunnel junction rings. Schematically shown are the layers of the (c) ring and (d) two stable magnetization patterns of one magnetic layer at zero magnetic field (remanent states): vortex (V) and onion (O) states. Note that there are other equivalent states that correspond to the reversal of the polarity of the magnetization of the above two states.

the V state. Our micromagnetic simulation[18] shows that the transition from the onion state to the vortex state does not occur when one just sweeps the in-plane magnetic field from a large positive value to a negative one for the samples with only 2.5 nm layer thickness. Instead, the two domain walls of the onion state rotate along the circumference until the polarization of the onion state is reversed. We will discuss the generation of the V state at the end of the paper.

A. Magnetic-field-driven switching

Figure 2 shows the tunnel resistance when we apply an in-plane magnetic field along the easy axis of the ring. At a large field, the magnetization of both rings are in the parallel onion state and, thus, the resistance is lowest. When the field is reduced, the stray field of the domain walls causes the onion states of the upper and lower rings to rotate oppositely in order to reduce the magnetostatic energy. Since the anisotropy of the two layers is small, each onion state will oppositely rotate by 90° to form an antiparallel configuration and the tunnel resistance becomes maximum. Further reversing the magnetic field causes the onion states of the two layers to become parallel again.

To reproduce the qualitative features of the above experimental data, we perform a numerical simulation by taking the following plausible assumptions. First, the several jumps shown in Fig. 2(a) indicate the existence of pinning potentials, and we model the pinning by simply including an in-plane fourfold anisotropic field. Second, an interlayer coupling between two rings is likely to exist for the ultrathin Al_2O_3 insulator barrier. Thus, we have added a 60 Oe ferromagnetic coupling field, which is consistent with our previous experiments on similar junctions having elliptical shapes.[19] Third, the tunnel conductance $G(H)$ is calculated via the standard formulation of tunnel magnetoresistance as follows:

$$G(H) = G_p - \frac{G_p - G_a}{2A} \int dxdy[1 - \cos\,\theta(x,y)], \qquad (1)$$

where G_p (G_a) are the conductance for the two magnetic layers in parallel (antiparallel), A is the area of the ring, $\theta(x,y)$ is the angle between the local magnetization vectors $\vec{M}_t(x,y)$ and $\vec{M}_b(x,y)$ of the top and bottom rings, and (x,y) denotes the in-plane coordinates. Once the magnetization states of the top and bottom rings are obtained via micromagnetic simulation, the conduction $G(H)$ or the tunnel magnetoresistance $R(H)=G^{-1}(H)$ can readily be derived from Eq. (1). As seen from Fig. 2(b), the simulated results reproduce the main shape of the experimental R-H curves.

We note that there are several subtle features that are not reproduced by the simulation. First, the gradual increase in the resistance at low field observed in the experiment indicates the gradual rotation of the domain walls; the origin is likely from the competition between magnetostatic interactions of the two rings and the pinning potentials.[20] Second, there are small sudden jumps in the resistance at low fields between the parallel resistance and the onset of the gradual increase to the antiparallel resistance. The reason might be due to the misalignment among the easy axes of the two layers and the direction of the magnetic field. If we consider

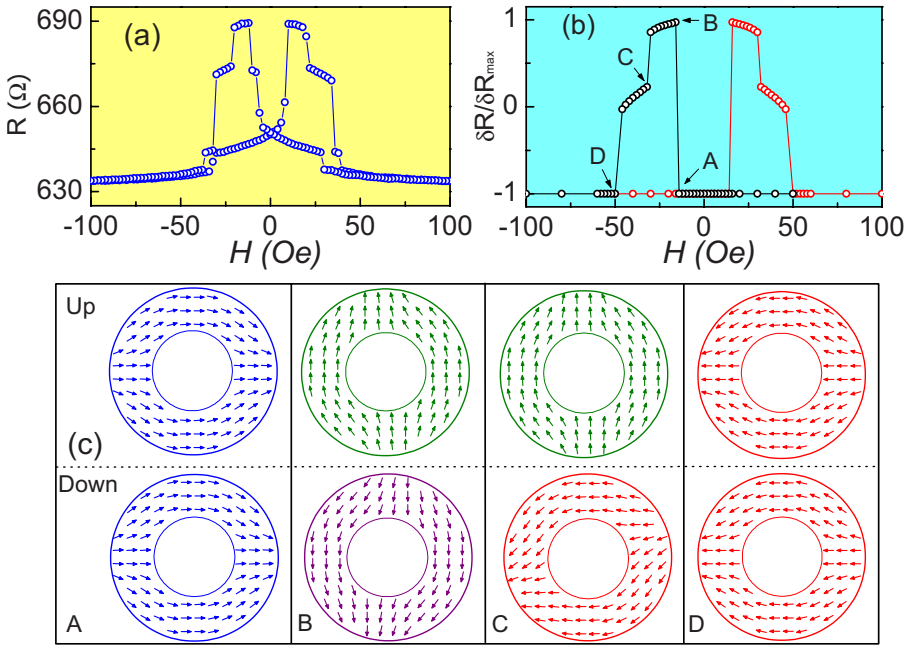

FIG. 2. (Color online) (a) The room-temperature tunnel resistance as a function of the magnetic field for a ring-shaped MTJ whose outer diameter is 100 nm. (b) Calculated normalized tunnel resistance $\delta R/\delta R_{max}$, where $\delta R=R(H)-R_p$, $\delta R_{max}=R_a-R_p$, and R_p and R_a are the resistances for the parallel and antiparallel aligned onion states of the top and bottom rings. The parameters in micromagnetic simulation are specified as below: the uniaxial anisotropy of FeCo is 50 Oe and that of FeCoB is 0, the saturation magnetizations of FeCo and FeCoB are 1130 and 1000 emu/cc, and the interlayer coupling field is 60 Oe. (c) In addition, an in-plane fourfold anisotropic field of 90 Oe is applied to mimic the pinning potentials.

that the easy axes of the two layers make an angle θ, a large field would make the onion states of the two layers parallel. As the field reduces to a smaller value, a transition occurs where the two onion states tend to return to their respective easy axis, i.e., form approximately an angle θ. Note that this irreversible jump depends on the location of the pinning potential. We show in Fig. 3 the *R-H* characteristic of a similar ring, where the major and minor hysteresis jumps occur in several magnetic fields. Interestingly, the inserted minor loop contains only one small jump. These uncontrolled subtle features indicate the imperfection of the ring structure.

B. Current-driven switching

Next, we show the tunnel resistance by sweeping the current at zero magnetic field. The data were recorded as follows. Before each resistance measurement, a current pulse with amplitude I and width of 200 ns was applied. The resistance is then measured by using a low readout current of 10 μA that will not disturb the magnetic state formed after each current pulse. By repeating the above process for an increasing or decreasing amplitude of I, we obtained the full *R-I* loop in Fig. 4. One notices that the two values of the resistance are very close to the values in Fig. 2(a), which indicates that the magnetization of the two layers are two onions states with parallel (low resistance) and antiparallel (high resistance) configurations. The critical switching current from antiparallel (parallel) to parallel (antiparallel) states is about 1.1 mA, which corresponds to the current density of about 6×10^6 A/cm^2.

Two competing mechanisms are responsible for the switching of the magnetization by the current. First, the current induces a circular magnetic field that may affect the magnetization states. However, our data suggest that the current-induced magnetic field cannot be the dominant mechanism for the switching: (1) for the current $I=1$ mA, the maximum Oersted field at the outer boundary of a 100-nm-diameter infinitely long cylinder is less than 40 Oe; this Oersted field is clearly an overestimation since the field would be smaller for our ring structure. Simulation indicates that one needs at least several times larger current density to

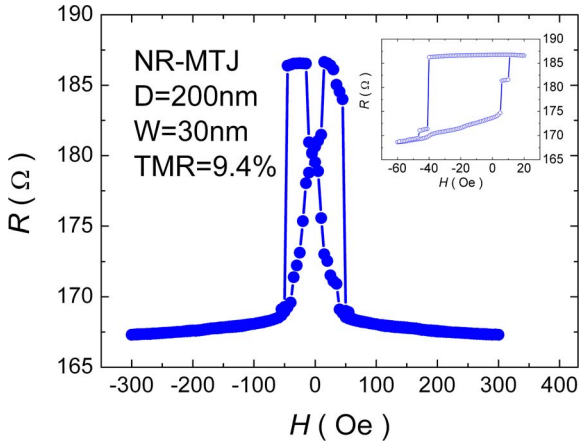

FIG. 3. (Color online) The room-temperature tunnel resistance as a function of the magnetic field for a ring-shaped MTJ whose outer diameter is 200 nm. Inset: The minor hysteresis loop.

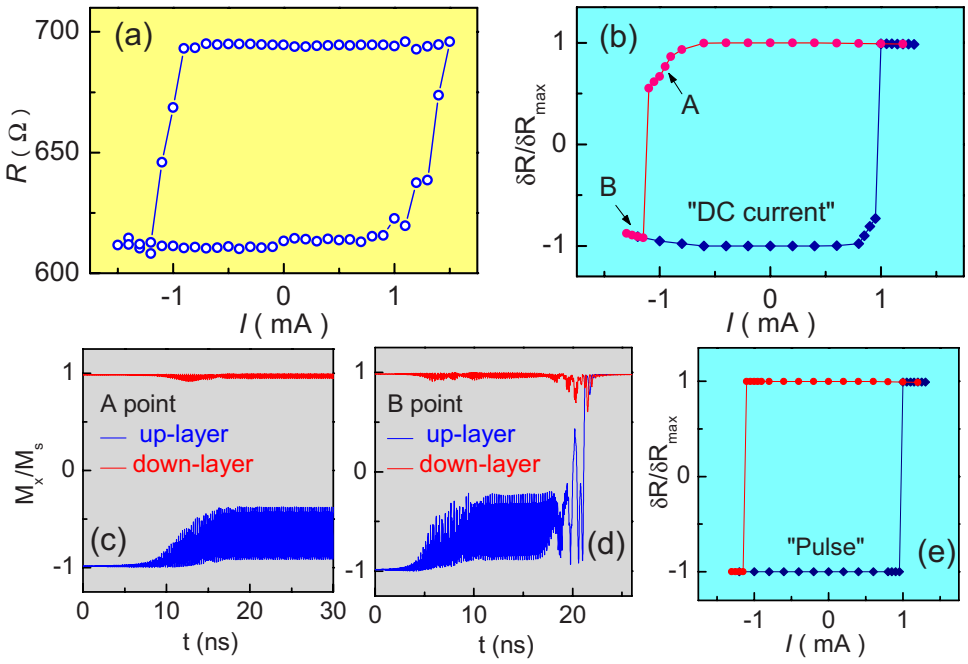

FIG. 4. (Color online) The tunnel resistance as a function of the amplitude of the 200 ns pulsed current density at zero magnetic field. (a) Experimental results at room temperature. Simulation results of the *R-I* loop: (b) the precessional states near the critical current density and (c) the switched state for the current exceeding the critical value. (d) The same set of parameters as in Fig. 2 in addition to the damping parameters of 0.01 and 0.015 for the top and bottom magnetic rings are used for the simulation. (e) The simulated *R-I* curve after the pulsed current is turned off.

reverse the polarity of the onion state. More specifically, we find from micromagnetic simulation that without the spin torque, the circular Oersted field is able to rotate the domain walls of the onion state by only a few degrees. (2) The measured critical current density, shown in Fig. 4(a), is approximately the same for different sizes of rings (not shown), while the Oersted-field-driven reversal[13] would be strongly size dependent. Thus, we propose that the spin transfer torque is the dominant factor for the observed switching.

We have performed micromagnetic simulation by explicitly taking into account both the spin torque and the induced Oersted field. We model the spin torque on $\mathbf{m}_i$ via $a_J \mathbf{m}_i \times (\mathbf{m}_i \times \mathbf{m}_j)$,[21] where a_J is proportional to the current. Figures 4(b)–4(e) show the simulation results. We note that both the observed [Fig. 4(a)] and simulated [Fig. 4(b)] *R-I* loops do not show distinct steps (see Fig. 2); this indicates that the current-driven switching is relatively insensitive to local pinnings as compared to the field-driven switching. We attribute this feature to the spin transfer torque: the switching current density I_c is proportional to $H_K + 2\pi M_s$, where H_K is the anisotropy field and M_s is the saturation magnetization.[14] Since $2\pi M_s$ is much larger than H_K and pinning potentials, the critical current is thus not sensitive to the local defects. We also notice that the simulation shows a gradual change in resistance just before switching near the parallel (antiparallel) resistance at positive (negative) currents, while the experimental switching between parallel and antiparallel resistances is abrupt. This discrepancy is due to an artifact, in which the simulation was carried out with a constant current density. When the current is near the switching current, one of the layers is in a stable precessional state (this stable precessional state is a signature of the spin torque) [see Fig. 4(c)]. Experimentally, the resistance was measured after the pulsed current was switched off. Therefore, the measured states returned to the parallel onion states. If we turn off the current after a certain time during the simulation, the loop will not change gradually because the precessional states will return to either the parallel or antiparallel state, [see Fig. 4(e)].

C. Discussions and summary

The quantitative analysis of the spin torque effect in MTJ involves a number of key parameters. The critical current at finite temperature is given by[22,23]

$$I_c = I_{c0}\left(1 - \frac{k_B T^*}{E_b} \ln(t_p f_0)\right), \tag{2}$$

where I_{c0} is the intrinsic (zero temperature) critical current, T^* is the temperature, E_b is the energy barrier separating the antiparallel and parallel onion states, $t_p = 200$ ns is the pulse width of the current, and $f_0 \approx 10^9\ \mathrm{s}^{-1}$ is the attempt frequency. It is expected that the temperature will be significantly higher than the room temperature when the bias voltage is of the order of 1 V.[24] The energy barrier depends on the detail of the magnetostatic interaction as well as the defects of the ring structure.[25,26] Furthermore, the recently proposed perpendicular spin torque also contributes to the energy barrier.[27,28] The uncertainty of these parameters makes the quantitative comparison very difficult, if not at all impossible. We show in Fig. 5 the critical current as a function of the temperature. The significant reduction of the critical cur-

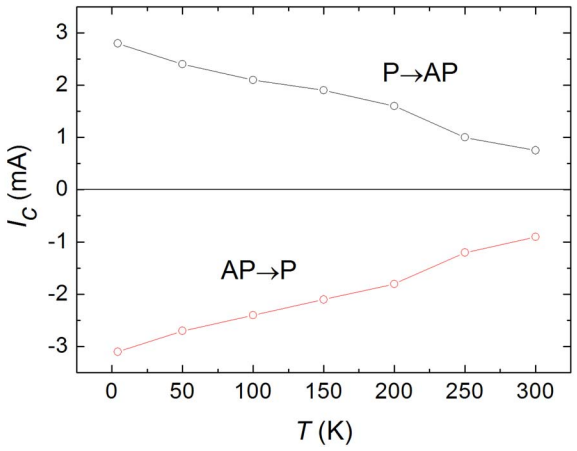

FIG. 5. (Color online) The temperature dependence of the dc critical current density for a ring-shaped MTJ whose outer diameter is 100 nm.

rent at high temperatures implies the importance of the thermally assisted switching.

While our initial motivation for the study of the ring structure is to create and switch vortex states that are robust against thermal fluctuation, we are unable to create such stable vortex states in the present experiments. A plausible interpretation is that the vortex states are topologically different from the onion states, and one needs to annihilate two magnetic domains of the onion state to create a vortex state. For our ultrathin rings, one would require a large out-of-plane rotation to convert the onion to the vortex states and, thus, it is energetically prohibited. One possible way to initialize a vortex state is to utilize a circular magnetic field generated by the current, but the required current density is too high. Other methods, for example, applying a large out-of-plane field along with a moderate current, might be more suitable for the initial formation of the vortex states. It is an experimentally challenging problem to manipulate well-controlled vortex states in ultrathin rings. We defer this study in the future.

In summary, we demonstrate that the magnetization of the ring-shaped MTJ can be switched by a current. The current density of the order of 6×10^6 A/cm^2 is sufficient to switch from one onion state to another. This work opens a possibility for creating high-density magnetic elements with enhanced thermal stability and reduced power consumption.

ACKNOWLEDGMENTS

This research was supported by the State Key Project of Fundamental Research of the Ministry of Science and Technology (MOST, No. 2006CB932200), the Chinese Academy of Sciences (CAS), and the National Natural Science Foundation (NSFC), China. X.F.H. gratefully acknowledges the partial support of the Outstanding Young Researcher Foundation (Grant No. 50528101 and Outstanding Innovation Team Foundation (Grant No. 50721001), NSFC project (Grant No. 10574156), the Wang Kuan-Cheng Foundation, and the Micro-fabrication Center of IOP from CAS. S.Z. acknowledges the support of the NSF (DMR-0704182) and the U.S. DOE (DE-FG02-06ER46307).

*Corresponding authors.
†xfhan@aphy.iphy.ac.cn
‡zhangshu@missouri.edu

[1] J. A. Katine, F. J. Albert, R. A. Buhrman, E. B. Myers, and D. C. Ralph, Phys. Rev. Lett. **84**, 3149 (2000).
[2] Y. Huai, F. Albert, P. Nguyen, M. Pakala, and T. Valet, Appl. Phys. Lett. **84**, 3118 (2004).
[3] J.-G. Zhu, Y. Zheng, and G. A. Prinz, J. Appl. Phys. **87**, 6668 (2000).
[4] C. L. Chien, F. Q. Zhu, and J. G. Zhu, Phys. Today **60**, 40 (2007).
[5] F. Q. Zhu, G. W. Chern, O. Tchernyshyov, X. C. Zhu, J. G. Zhu, and C. L. Chien, Phys. Rev. Lett. **96**, 027205 (2006).
[6] C. A. F. Vaz *et al.*, J. Phys.: Condens. Matter **19**, 255207 (2007), and references therein.
[7] S. P. Li, D. Peyrade, M. Natali, A. Lebib, Y. Chen, U. Ebels, L. D. Buda, and K. Ounadjela, Phys. Rev. Lett. **86**, 1102 (2001).
[8] J. Rothman, M. Klaui, L. Lopez-Diaz, C. A. F. Vaz, A. Bleloch, J. A. C. Bland, Z. Cui, and R. Speaks, Phys. Rev. Lett. **86**, 1098 (2001).
[9] W. Jung, F. J. Castano, and C. A. Ross, Appl. Phys. Lett. **91**, 152508 (2007).
[10] F. J. Castano, D. Morecroft, W. Jung, and C. A. Ross, Phys. Rev. Lett. **95**, 137201 (2005).
[11] T. Yang, A. Hirohata, M. Hara, T. Kimura, and Y. Otani, Appl. Phys. Lett. **90**, 092505 (2007).
[12] M. T. Moneck and J. -G. Zhu, J. Appl. Phys. **99**, 08H709 (2006).
[13] C. C. Chen, C. C. Chang, Y. C. Chang, C. T. Chao, C. Y. Kuo, Lance Horng, J. C. Wu, Teho Wu, G. Chern, C. Y. Huang, M. Tsunoda, and M. Takahashi, IEEE Trans. Magn. **43**, 920 (2007).
[14] J. C. Slonczewski, J. Magn. Magn. Mater. **159**, L1 (1996).
[15] Z. C. Wen, H. X. Wei, and X. F. Han, Appl. Phys. Lett. **91**, 122511 (2007).
[16] Z. M. Zeng, J. F. Feng, Y. Wang, X. F. Han, W. S. Zhan, X. G. Zhang, and Z. Zhang, Phys. Rev. Lett. **97**, 106605 (2006).
[17] Hong-Xiang Wei, Mark C. Hickey, Graham I. R. Anderson, Xiu-Feng Han, and Christopher H. Marrows, Phys. Rev. B **77**, 132401 (2008).
[18] Zero-temperature micromagnetic simulation is carried out by choosing the mesh size $5\times5\times0.8$ nm^3 so that there are a total of seven meshes in the thickness dimension (the center layer is Al_2O_3, which does not have a magnetic moment) throughout the paper. Special care is taken for the edges of the rings; see M. J. Donahue and R. D. McMichael, IEEE Trans. Magn. **43**, 2878 (2006).
[19] X. F. Han, S. F. Zhao, and A. C. C. Yu, Sci. Technol. Adv. Mater. **6/7**, 784 (2005).
[20] T. J. Hayward, J. Llandro, R. B. Balsod, J. A. C. Bland, D. Morecroft, F. J. Castano, and C. A. Ross, Phys. Rev. B **74**, 134405 (2006).

[21] Z. Li and S. Zhang, Phys. Rev. B **68**, 024404 (2003).
[22] R. H. Koch, J. A. Katine, and J. Z. Sun, Phys. Rev. Lett. **92**, 088302 (2004).
[23] Z. Li and S. Zhang, Phys. Rev. B **69**, 134416 (2004).
[24] M. Yoshikawa, T. Ueda, H. Aikawa, N. Shimomura, E. Kitagawa, M. Nakayama, T. Kai, K. Nishiyama, T. Nagase, T. Kishi, S. Ikegawa, and H. Yoda, J. Appl. Phys. **101**, 09A511 (2007).
[25] E. Martinez, L. Lopez-Diaz, O. Alejos, L. Torres, and C. Tristan, Phys. Rev. Lett. **98**, 267202 (2007).
[26] J. He, Z. Li, and S. Zhang, J. Appl. Phys. **98**, 016108 (2005).
[27] J. C. Slonczewski and J. Z. Sun, J. Magn. Magn. Mater. **310**, 169 (2007).
[28] I. Theodonis, N. Kioussis, A. Kalitsov, M. Chshiev, and W. H. Butler, Phys. Rev. Lett. **97**, 237205 (2006).